

Au and Fe magnetic moments in disordered Au-Fe alloys

F. Wilhelm,¹ P. Pouloupoulos,^{2,*} V. Kapaklis,^{2,3} J.-P. Kappler,⁴ N. Jaouen,^{1,†} A. Rogalev,¹ A. N. Yaresko,⁵ and C. Politis^{3,6}

¹European Synchrotron Radiation Facility (ESRF), B. P. 220, 38043 Grenoble, France

²Materials Science Department, University of Patras, 26504 Patras, Greece

³School of Engineering, Engineering Science Department, University of Patras, 26504 Patras, Greece

⁴Institut de Physique et Chimie des Matériaux de Strasbourg (IPCMS), 23 rue du Loess, 67037 Strasbourg, France

⁵Max Planck Institute for the Physics of Complex Systems, D-01187 Dresden, Germany

⁶Forschungszentrum Karlsruhe, Institut für Nanotechnologie, P.O. Box 3640, 76021 Karlsruhe, Germany

(Received 18 January 2008; revised manuscript received 27 April 2008; published 9 June 2008)

We report on the magnetic moments of Au and Fe in fcc and bcc disordered Au-Fe alloys determined via a combination of x-ray magnetic circular dichroic measurements at the $L_{3,2}$ edges of Au and superconducting quantum interference device magnetometry. The $5d$ induced magnetic moment of Au in the fcc alloys scales with the number N of nearest Fe neighbors, from $M_{\text{Au}}=0.1 \mu_B/\text{atom}$ for $N=3$ to $M_{\text{Au}}=0.2 \mu_B/\text{atom}$ for $N=6$. Fe in these alloys is in a high-spin state, which carries a total magnetic moment of about $3 \mu_B/\text{atom}$. The maximum value of $5d$ induced magnetic moment of Au is $0.33 \mu_B/\text{atom}$ and is exhibited when Au is placed as an impurity in a bcc Fe environment. The ratio of the orbital-to-spin $5d$ magnetic moment of Au is $M_L/M_S \approx 0.2$ in all samples. The experimental results are discussed with respect to first principles calculations.

DOI: [10.1103/PhysRevB.77.224414](https://doi.org/10.1103/PhysRevB.77.224414)

PACS number(s): 75.50.Bb, 78.70.Dm, 75.30.Cr

I. INTRODUCTION

Technological progress in third generation synchrotron radiation facilities has made possible nowadays the element-specific determination of magnetic moments in multielement materials.¹ Even very small magnetic moment contributions in such materials can be measured with high precision. A recent example is the magnetic moment of Au investigated by x-ray magnetic circular dichroism (XMCD) experiments. Au was shown to acquire a small induced magnetic moment in the range of $0.03\text{--}0.06 \mu_B/\text{atom}$ at interfaces with Co in Co/Au multilayers.² Successive works have demonstrated that even self-organized Au nanoparticles may have, when placed in specific organic environments, some small magnetic moment.^{3,4}

In this work, we focus on the Au and Fe magnetic moments in disordered Au-Fe alloys. This system has been extensively studied for the last four decades because it presents a rich variety of interesting structural and magnetic properties. In the low Fe concentration limit, (below about 16 at. % Fe) fcc Au-Fe alloys show a paramagnetic to spin-glass transition by lowering the temperature. In the concentration interval of 16–24 at. % Fe, Au-Fe alloys exhibit double transitions between ferromagnetic and spin-glass phases as a function of temperature (“reentrant” spin-glass behavior).^{5–7} When the Fe concentration is larger than about 24 at. %, Au-Fe alloys become regular ferromagnets. For concentrations up to 53 at. % Fe, fcc Au-Fe alloys are quite easily stabilized at room temperature despite the fact that the fcc phase is only a high temperature phase according to the binary alloy phase diagram of the Au-Fe system.⁸ Already since the 70s, Cable and Wollan,⁹ via measuring the magnetic form factors of fcc $\text{Au}_{75}\text{Fe}_{25}$ disorder alloys, have provided a magnetic moment of $2.84 \mu_B/\text{atom}$ for Fe and an upper limit of $0.03 \mu_B/\text{atom}$ for Au. One may understand the large magnetic moment of Fe as a magnetovolume effect. Indeed, successive tight binding calculations showed

that fcc Fe should present a high-spin state upon volume expansion.¹⁰ Fe-rich alloys are encountered in the normal bcc (α -Fe) phase. In this phase, the magnetic moment of Fe is $2.2 \mu_B/\text{atom}$.¹¹ An early XMCD experiment on bcc $\text{Au}_3\text{Fe}_{97}$ alloys yield for the $5d$ magnetic moment of Au a value of less than $0.1 \mu_B/\text{atom}$ for Au, while, interestingly, in the same publication, first principles calculations predicted $0.3 \mu_B/\text{atom}$.¹²

In the present work, we determine the total magnetic moment of Fe and the $5d$ magnetic moment of Au for the disordered fcc and bcc Au-Fe alloys in the concentration range of 25–97 at. % Fe, via a combination of XMCD and superconducting quantum interference device (SQUID) magnetometries. The results are discussed with the help of fully relativistic first principles calculations. We confirm the existence of the high-spin Fe state in the fcc regime. We find that Au has a sizeable $5d$ orbital magnetic moment, which is about 20% as large as its spin magnetic moment for all samples. Considerable induced $5d$ magnetic moments are revealed for Au and increase with the number of nearest Fe neighbors. The maximum value of the induced $5d$ magnetic Au moment $\mu_{\text{Au}}=0.33 \mu_B/\text{atom}$ is exhibited when Au is in impurity form, totally surrounded by Fe neighbors in bcc Au-Fe alloys. The experimental results are in a satisfactory agreement with our first principles calculations.

II. EXPERIMENTAL AND COMPUTATIONAL DETAILS

$\text{Au}_{50}\text{Fe}_{50}$ (sample A), $\text{Au}_{75}\text{Fe}_{25}$ (sample B), and $\text{Au}_3\text{Fe}_{97}$ (sample C) alloys were prepared in bulk form by arc melting under 600 mbar argon atmosphere. (Indices denote concentration in at. %.) The structure of the samples was determined by x-ray diffraction (XRD). The measurements were performed with the help of a standard powder diffractometer (SEIFFERT) with the Ni-filtered $\text{Cu } K\alpha_1$ radiation ($\lambda = 0.15405 \text{ nm}$). Samples A and B were shown to be in a single fcc phase. Au and Fe may form fcc solid solutions in

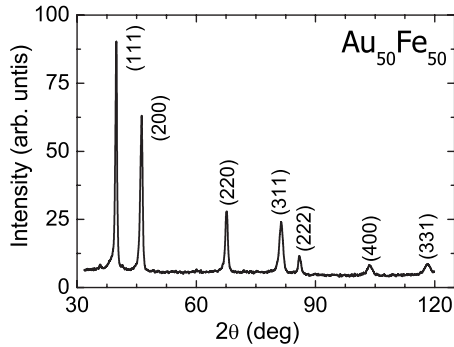


FIG. 1. X-ray diffraction pattern from an $\text{Au}_{50}\text{Fe}_{50}$ alloy (sample A). All diffraction peaks are labeled. The pattern provides clear evidence for a fcc single-phase solid solution.

a broad composition range at relatively elevated temperatures, according to the binary alloy phase diagram of this system.⁸ By quenching, one may stabilize the fcc phase at room temperature even though the thermodynamically favored phase at room temperature is the bcc one.⁸ According to the phase diagram, the maximum Fe concentration for which this recipe may safely work is 53 at. % Fe. In Fig. 1, we plot the XRD pattern for sample A. All diffraction peaks are identified solely with respect to the fcc crystallographic planes. The lattice constant which can be determined by this pattern via Bragg's law is $a=0.393$ nm. This value is 3.7% smaller than the lattice constant of bulk Au and 8% larger than the one of γ -Fe due to the formation of the solid solution. On the other hand, for sample C, the regular bcc Fe diffraction peaks were recorded.

SQUID magnetometry measurements were performed at a temperature $T=4$ K and under maximum external field of 5 T. The XMCD experiments were performed at the European Synchrotron Radiation Facility (ESRF) in Grenoble (France) on the ID12 beamline¹³ at the $L_{3,2}$ edges of Au using a highly efficient fluorescence yield detection mode in a backscattering geometry. The degree of polarization of the circular light provided by an apple-II type helical undulator HU38 after the monochromator equipped with a pair of Si(111) crystals was nearly 98%. In order to ensure complete magnetic saturation, magnetic fields that are much larger than the saturation field were applied. X-ray absorption (XAS) spectra were recorded at 4 K. The spectra have been corrected for self-absorption and saturation effects. To exclude any experimental artifacts, the XMCD spectra were recorded either by changing the helicity of the incoming light or by inverting the direction of the external applied magnetic field. A fcc Au foil was measured as a reference under the same experimental conditions.

The electronic structure of the alloys was self-consistently calculated on the basis of the local spin density approximation¹⁴ to the density functional theory using the fully relativistic spin-polarized linear muffin tin orbital (LMTO) method^{15–17} in the atomic-sphere approximation, including the combined correction (ASA+CC).^{15,18} Core-charge densities were calculated at every iteration of the self-consistency loop. The spin polarization was included in the variational step.¹⁹ The basis consisted of s , p , d , and f LMTOs for both Fe and Au. More details on the computa-

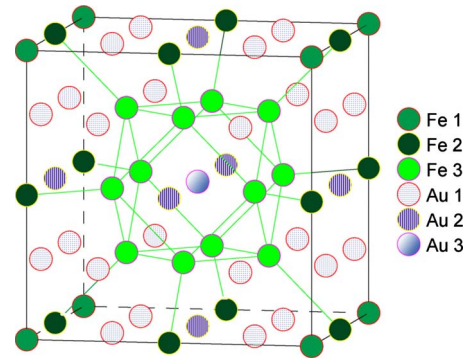


FIG. 2. (Color online) Unit cell employed in the *first principles* band structure calculations for a disordered fcc $\text{Au}_{50}\text{Fe}_{50}$ alloy. The numbering indicates the three different types, from point of view of symmetry, of Au and Fe atoms in the unit cell.

tional method may be found in Ref. 20. The disorder alloy structures were simulated by considering a large unit cell with many Fe and Au atoms placed in random positions as seen in Fig. 2 for the case of $\text{Au}_{50}\text{Fe}_{50}$. The lattice parameter $a=0.393$ nm was determined by the XRD spectra (see Fig. 1). Similar approaches were also applied for the calculations for samples B and C.

III. RESULTS AND DISCUSSION

A. Au spectra and magnetic moments

In Fig. 3, the XAS and the XMCD spectra at the $L_{3,2}$ edges of Au are plotted for sample A. For the XAS spectra, the ratio of the L_3/L_2 was normalized to 2.24/1 according to Ref. 21. The sizeable XMCD signal reveals that Au has acquired an induced magnetic moment. By knowing the direction of the magnetic field and the helicity of the beam, we conclude that Au is polarized parallel to the Fe magnetic moment. In order to determine the magnetic moment of Au and disentangle it into spin and orbital contributions, we have applied the sum-rule analysis.²² For the evaluation of

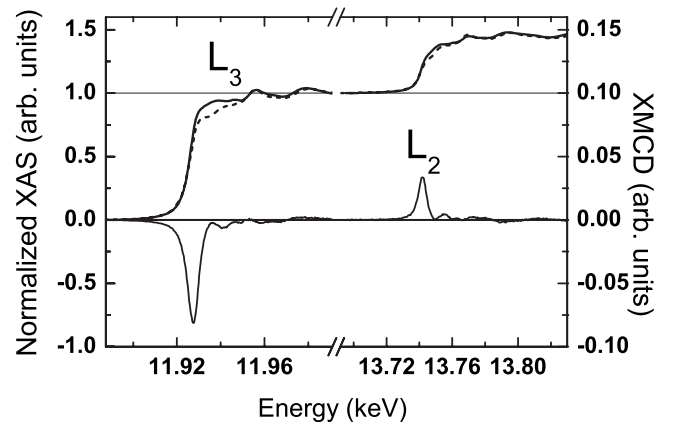


FIG. 3. X-ray absorption (top, solid line) and x-ray magnetic circular dichroism (bottom) spectra recorded at the $L_{3,2}$ edges of Au in a fcc $\text{Au}_{50}\text{Fe}_{50}$ solid solution. The corresponding XAS spectra of a reference fcc Au foil have been also included (top, dashed line).

the number n_h of $5d$ holes of Au in the alloys, we have followed a similar process as the one described in Ref. 23, i.e., we compared the white line intensities to the one of a reference fcc Au foil. For the Au foil, $n_{\text{href}}=0.688$.^{2,24} This comparison shows that the so-called “white line” intensity for pure Au is very small, however, it is not equal to zero. This originates from the presence of unoccupied states of $d_{5/2}$ and $d_{3/2}$ character in the vicinity of the Fermi level due to s - p - d hybridization.²⁵ Obviously, there is an increase in the white line of Au with the presence of Fe. This white line increase may be interpreted as an increase in the number of $5d$ holes for Au. On the other hand, at the L_2 edge, this effect is much less pronounced, which indicates that the presence of Fe mostly influences the $d_{3/2}$ states.

For the evaluation of the $5d$ magnetic moments of Au, we have used the following information from our first principles calculations: Our calculations have shown that the expectation value of the T_Z term in all samples is less than 1% of the S_z . We also feel important to underline that $p \rightarrow s$ transitions are also allowed at the L edges and need, in principle, to be taken into account. Our calculation showed, however, that $p \rightarrow s$ transitions are at least two orders of magnitude smaller than the $p \rightarrow d$ transitions. Moreover, quadrupolar transitions at the L edges ($p \rightarrow p$ and $p \rightarrow f$) are also expected to be much smaller than dipolar ones. Therefore, all the aforementioned contributions were neglected in our analysis for the evaluation of the $5d$ moment of Au. Our analysis resulted in the following values for the $5d$ magnetic moments of Au: $M_{\text{Au}}=0.20 \mu_B/\text{atom}$ and $M_L/M_S=0.21$. The same analysis for sample B resulted in $M_{\text{Au}}=0.10 \mu_B/\text{atom}$ and $M_L/M_S=0.21$.

For the bcc sample C, we have followed a different technique in the analysis. The reason is that the shape of the XAS spectra is strongly influenced by the local crystallographic symmetry, so the fcc Au reference XAS do not match to the ones in the sample. In such a case, we follow the same approximate method, which we have recently adopted for a similar case in CoCrPt alloys.^{26,27} That is, after normalizing the XAS spectra, we compared the XMCD spectra of Au in the sample C directly to the ones of Au in the fcc alloys (see Fig. 4). This idea is justified by the fundamental principle that the sum rules establish a simple linear relationship between the magnitude of XMCD signal and the magnetic moment (for a detailed discussion, see Ref. 28). This analysis yields the following values for the $5d$ moments of Au: $M_{\text{Au}}=0.33 \mu_B/\text{atom}$ and $M_L/M_S=0.18$. In Fig. 4, the XMCD spectra recorded at the $L_{3,2}$ edges of Au in Au-Fe alloys are plotted in order to visualize in a direct way the increase in the induced magnetic moment of Au with Fe concentration. By comparing the results for the three samples, one may see that the $5d$ magnetic moment of Au seems to strongly depend and to be almost proportional to the number N of nearest neighboring Fe atoms. Such a behavior is not universal, however. It has been observed also for induced magnetic moments in other binary alloys over wide concentration intervals, see e.g., Ref. 29 for NiPt alloys. On the other hand, the XMCD spectral shape is similar for all samples at both $L_{3,2}$ edges.

These considerable magnetic moment values for Au may be thought that they are in quite some conflict with early

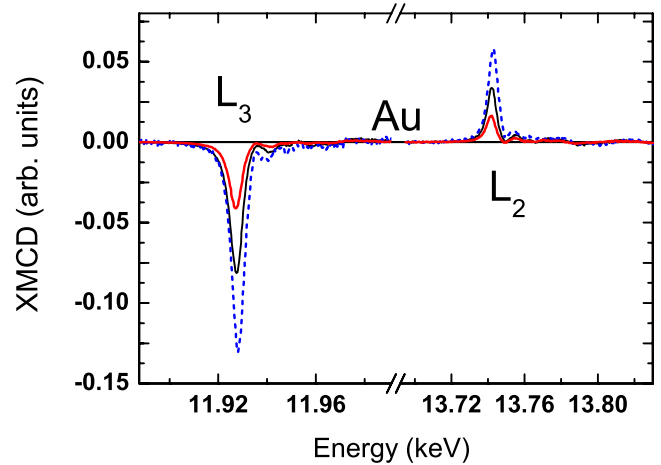


FIG. 4. (Color online) XMCD spectra at the $L_{3,2}$ edges of Au in bcc $\text{Au}_3\text{Fe}_{97}$ alloy (dashed), fcc $\text{Au}_{50}\text{Fe}_{50}$ alloy (thin solid), and fcc $\text{Au}_{75}\text{Fe}_{25}$ alloy (thick solid line).

experiments providing an upper limit of $0.03 \mu_B/\text{atom}$ for fcc $\text{Au}_{75}\text{Fe}_{25}$ alloys.⁹ However, while XMCD measurements at the $L_{3,2}$ edges of Au provide the $5d$ induced magnetic moment for Au due to the selection rules, which practically allow only transitions with $\Delta l = \pm 1$, the total magnetic moment of Au consists of $6s$, $6p$, and $5d$ of contributions (see also a detailed discussion in Ref. 30). Therefore, it was necessary to perform first principles calculations and compare the results to the experiment. The calculated values are listed together with experimental ones in Table I. Calculation yields a magnetic moment carried out by the $5d$ orbitals of Au to be $0.15 \mu_B/\text{atom}$ in sample A and $\mu_{\text{Au}}=0.066 \mu_B/\text{atom}$ in sample B. These values are in reasonable agreement to the experimental ones. The ratio of the induced $5d$ Au magnetic moments in the two alloys is of about 2, as in the experiment. Interestingly, due to the negative $6s$ and $6p$ contributions, the total magnetic moment of Au is only $0.076 \mu_B/\text{atom}$ for sample A and $0.033 \mu_B/\text{atom}$ for sample B. Thus, one may see that the total induced magnetic moment of Au in $\text{Au}_{75}\text{Fe}_{25}$ is very close to the experimental result of Ref. 9. The ratios $M_L/M_S=0.25$ for sample A and 0.24 for sample B are in very good agreement with the experimentally determined value of 0.21. Finally, for sample C, the experimental value for the $5d$ magnetic moment of Au is also in good agreement with the corresponding ones of $0.29 \mu_B/\text{atom}$ (Ref. 12) and of $0.4 \mu_B/\text{atom}$ (Ref. 31), which resulted from previous first principles calculations. Our own first principles calculation yields $\mu_{\text{Au}}=0.32 \mu_B/\text{atom}$ and $\mu_L/\mu_S=0.20$, which is in excellent agreement with the experiment. On the other hand, Ref. 12 provides a $\mu_L/\mu_S=0.3$ value, which is quite larger than our experimental one.

B. Fe magnetic moments

In order to determine the Fe magnetic moments, we have followed the same method, which was adopted earlier for Fe/V superlattices³² and FeBY alloys.³³ Namely, we have performed SQUID magnetometry measurements and, suc-

TABLE I. Experimental and calculated magnetic moments for Au-Fe alloys. The magnetic moments are expressed in μ_B/atom units. The error bars in the analysis are of about $\pm 10\%$.

Sample	Total	s	p	d	d_{exp}	Total _{exp}
A (Au ₅₀ Fe ₅₀)						
Au						
M_S	0.0423	-0.0255	-0.0526	0.121	0.163	
M_L	0.0336	0	0.0047	0.029	0.034	
M_L+M_S	0.0763	-0.0255	-0.0479	0.150	0.197	
Fe						
M_S	2.813	0.0043	-0.0109	2.820		
M_L	0.054	0	-0.0000	0.054		
M_S+M_L	2.867	0.0043	-0.01093	2.874		2.90
B (Au ₇₅ Fe ₂₅)						
Au						
M_S	0.0180	-0.0153	-0.0200	0.0533	0.082	
M_L	0.0148	0	0.0019	0.0129	0.017	
M_S+M_L	0.0328	-0.0153	-0.0181	0.0662	0.099	
Fe						
M_S	3.051	0.0218	0.0148	3.015		
M_L	0.0835	0	-0.0005	0.084		
M_S+M_L	3.135	0.0218	0.0143	3.099		3.01
C (Au ₃ Fe ₉₇)						
Au						
M_S	0.1800	-0.0180	-0.0730	0.271	0.280	
M_L	0.0591	0	0.0060	0.053	0.050	
M_S+M_L	0.2392	-0.0180	-0.0670	0.324	0.330	
Fe						
M_S	2.398	-0.0095	-0.0394	2.447		
M_L	0.055	0	-0.0002	0.055		
M_S+M_L	2.453	-0.0095	-0.0396	2.502		2.2 ^a

^aReference 11.

cessively, we subtracted from the total magnetization signal the Au contribution, as obtained by combining the information from the XMCD data and our own first principles calculations. For this latter purpose, we have taken the ratio of the total-to- $5d$ moment contribution from the first principles calculations and we scaled the moment value determined by the XMCD accordingly. In Fig. 5, the magnetization curves for the fcc samples A and B are plotted. If one normalizes to the number of the nominally magnetic atoms only, which is Fe, as it is frequently done in the case of multielement materials, see discussions in Ref. 34, one yields values of $M_{\text{Fe}} = 3.0$ and $3.16 \mu_B/\text{atom}$, respectively, for samples A and B. By taking into account, however, the magnetic contribution of Au, as aforementioned, the corresponding Fe magnetic moments should be $\mu_{\text{Fe}} = 2.90$ and $3.01 \mu_B/\text{atom}$. These large values clearly indicate that Fe is in the high-spin magnetic state. On the other hand, for the Fe-rich bcc sample C, the magnetic moment of Fe shown in Table I has been reasonably considered to be equal to the one of bulk Fe.¹¹ The main results on the Au and Fe magnetic moments from Table I are plotted in Fig. 6 in order for the various trends of the

magnetic moments as a function of Fe concentration to be easily viewed.

The Fe moment for the Au₇₅Fe₂₅ sample is in very good agreement with the early experiments of Ref. 9. Reference

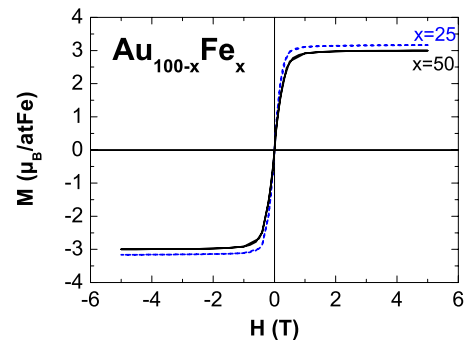


FIG. 5. (Color online) Magnetization curves for two fcc Au_{100-x}Fe_x alloys, as indicated, which are recorded by SQUID magnetometry at 4 K. The total magnetization is divided by the number of Fe atoms.

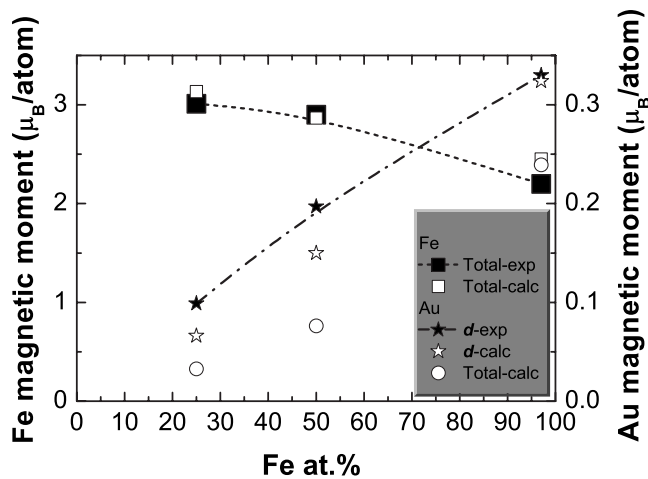


FIG. 6. Au and Fe magnetic moments as a function of the Fe concentration in disordered Au-Fe alloys. The lines are guides to the eye.

³¹ theoretically provides determined values $\mu_{\text{Fe}}=2.8$ and $3.2 \mu_{\text{B}}/\text{atom}$ for the $\text{Au}_{50}\text{Fe}_{50}$ and $\text{Au}_{75}\text{Fe}_{25}$ alloys, respectively, which reasonably agree well with our experiment. Our own first principles calculations for the two alloys, considering the experimentally determined lattice parameters, yield the values of $\mu_{\text{Fe}}=2.87$ and $3.13 \mu_{\text{B}}/\text{atom}$, respectively, which are in very good agreement with the experiment. The high-spin magnetic state of Fe has been also observed recently in tetragonal artificial Fe/Au superlattices³⁵ and this result has been successfully described by first principles calculations.³⁰

For the fcc Au-Fe samples, it is worth to notice the following: At first glance, one could be puzzled by the fact that by decreasing the Fe concentration, the magnetic moment of Fe increases. In Ni/Pt alloys²⁹ and multilayers,³⁶ as well as in FeV alloys³⁷ and superlattices,³² for example, the Ni or Fe magnetic moment decreases by decreasing the Ni or Fe con-

centration, respectively, and, finally, vanishes. This occurs because the number of “nonmagnetic” nearest neighbors around Ni or Fe, respectively, increases. The inverse behavior in Fe in the fcc Au-Fe alloys could be related to the expansion of the volume of the unit cell as the Fe (Au) concentration decreases (increases) in agreement with the pioneer theoretical calculations of Ref. 10. Successive first principles calculations have shown that microscopically, the increasing Au content results in a narrowing of the $3d$ band of Fe and to higher spin moments which could be reach up to $3.4 \mu_{\text{B}}/\text{atom}$ for Fe impurities in Au; a value which is very close to the limit of $4 \mu_{\text{B}}/\text{atom}$ for atomiclike Fe.³¹ Similarly, the high-spin state of Fe in tetragonal Fe/Au ordered alloys has been attributed to a considerable narrowing of the Fe density of states near the Fermi level because of the decreased number of nearest neighbors in these alloys as compared to the bulk. In that case, the majority spin $3d$ band of Fe becomes fully occupied and an enhanced magnetic moment is observed.^{19,30}

IV. SUMMARY

In summary, $5d$ spin, orbital, and total magnetic moments of Au in disordered fcc and bcc Au-Fe alloys were directly probed by x-ray magnetic circular dichroism. The $5d$ magnetic moments of Au are more than three times larger than the ones that early experiments have yielded. Combination with SQUID magnetometry enabled us to determine the magnetic moment of Fe and confirm a high-spin state of Fe in the fcc Au-Fe alloys. The magnetic moments of both Au and Fe are found in satisfactory agreement with the results of first principles calculations.

ACKNOWLEDGMENTS

We thank the ESRF crew for the excellent operational conditions. Financial support was partly provided by the ESRF.

*Corresponding author. FAX 997255; poulop@upatras.gr

[†]Present address: Synchrotron SOLEIL, L’Orme des Merisiers, 91192 Gif/Yvette, France.

¹P. Poulopoulos, A. Scherz, F. Wilhelm, H. Wende, and K. Baberschke, *Phys. Status Solidi A* **189**, 293 (2001).

²F. Wilhelm, M. Angelakeris, N. Jaouen, P. Poulopoulos, E. Th. Papaioannou, Ch. Mueller, P. Fumagalli, A. Rogalev, and N. K. Flevaris, *Phys. Rev. B* **69**, 220404(R) (2004).

³P. Crespo, R. Litran, T. C. Rojas, M. Multigner, J. M. de la Fuente, J. C. Sanchez-Lopez, M. A. Garcia, A. Hernando, S. Penades, and A. Fernandez, *Phys. Rev. Lett.* **93**, 087204 (2004).

⁴Y. Yamamoto, T. Miura, M. Suzuki, N. Kawamura, H. Miyagawa, T. Nakamura, K. Kobayashi, T. Teranishi, and H. Hori, *Phys. Rev. Lett.* **93**, 116801 (2004).

⁵B. H. Verbeek and J. A. Mydosh, *J. Phys. F: Met. Phys.* **8**, L109 (1978).

⁶I. A. Campbell, S. Senoussi, F. Varret, J. Teillet, and A. Hamzic, *Phys. Rev. Lett.* **50**, 1615 (1983); I. A. Campbell, D. Arvanitis,

and A. Fert, *ibid.* **51**, 57 (1983).

⁷I. A. Campbell, H. Hurdequint, and F. Hippert, *Phys. Rev. B* **33**, 3540 (1986).

⁸*Binary Alloy Phase Diagrams*, edited by T. B. Massalski (ASM International, Materials Park, OH, 1996).

⁹J. W. Cable and E. O. Wollan, *Phys. Rev. B* **7**, 2005 (1973).

¹⁰V. L. Moruzzi, P. M. Marcus, K. Schwarz, and P. Mohn, *Phys. Rev. B* **34**, 1784 (1986).

¹¹Ch. Kittel, *Introduction to Solid State Physics* (Wiley, New York, 1976).

¹²G. Schütz, M. Knülle, and H. Ebert, *Phys. Scr.*, T **49**, 302 (1993); H. Ebert, R. Zeller, B. Drittler, and P. H. Dederichs, *J. Appl. Phys.* **67**, 4576 (1990).

¹³A. Rogalev, J. Goulon, C. Goulon-Ginet, and C. Malgrange, in *Magnetism and Synchrotron Radiation*, Lecture Notes in Physics Vol. 565, edited by E. Beaurepaire, F. Scheurer, G. Krill, and J.-P. Kappler (Springer-Verlag, Berlin, 2001), p. 60.

¹⁴U. von Barth and L. A. Hedin, *J. Phys. C* **5**, 1629 (1972).

- ¹⁵O. K. Andersen, Phys. Rev. B **12**, 3060 (1975).
- ¹⁶V. V. Nemoshkalenko, A. E. Krasovskii, V. N. Antonov, V. N. Antonov, U. Fleck, H. Wonn, and P. Ziesche, Phys. Status Solidi B **120**, 283 (1983).
- ¹⁷V. N. Antonov, A. Ya. Perlov, A. P. Shpak, and A. N. Yaresko, J. Magn. Magn. Mater. **146**, 205 (1995).
- ¹⁸V. V. Nemoshalenko and V. N. Antonov, *Computational Methods in Solid State Physics* (Gordon and Breach, London, 1998).
- ¹⁹H. Ebert, Phys. Rev. B **38**, 9390 (1988).
- ²⁰S. Uba, L. Uba, A. N. Yaresko, A. Ya. Perlov, V. N. Antonov, and R. Gontarz, Phys. Rev. B **53**, 6526 (1996).
- ²¹<http://physics.nist.gov/PhysRefData/FFast/Text/cover.html>
- ²²B. T. Thole, P. Carra, F. Sette, and G. van der Laan, Phys. Rev. Lett. **68**, 1943 (1992); P. Carra, B. T. Thole, M. Altarelli, and X.-D. Wang, *ibid.* **70**, 694 (1993).
- ²³W. Grange, M. Maret, J.-P. Kappler, J. Vogel, A. Fontaine, F. Petroff, G. Krill, A. Rogalev, J. Goulon, M. Finazzi, and N. B. Brookes, Phys. Rev. B **58**, 6298 (1998).
- ²⁴A. Ya Perlov (unpublished).
- ²⁵C. C. Tyson, A. Bzowski, P. Kristof, M. Kuhn, R. Sammynaiken, and T. K. Sham, Phys. Rev. B **45**, 8924 (1992).
- ²⁶P. Pouloupoulos, F. Wilhelm, V. Kapaklis, N. Jaouen, M. Angelakeris, A. Rogalev, and C. Politis, Phys. Status Solidi A **201**, 3243 (2004).
- ²⁷P. Pouloupoulos, Int. J. Mod. Phys. B **19**, 4517 (2005).
- ²⁸A. Rogalev, F. Wilhelm, N. Jaouen, J. Goulon, and J.-P. Kappler, in *Magnetism: Synchrotron Radiation Approach*, Lecture Notes in Physics Vol. 697, edited by E. Beaurepaire, H. Bulou, F. Scheurer, and J.-P. Kappler (Springer-Verlag, Berlin, 2006), p. 83.
- ²⁹R. E. Parra and J. W. Cable, Phys. Rev. B **21**, 5494 (1980).
- ³⁰L. Uba, S. Uba, V. N. Antonov, A. N. Yaresko, T. Slezak, and J. Korecki, Phys. Rev. B **62**, 13731 (2000).
- ³¹B. Sanyal, P. Biswas, T. Saha-Dasgupta, A. Mookerjee, Ain-ul Huda, N. Choudhury, M. Ahmed, and A. Halder, J. Phys.: Condens. Matter **11**, 1833 (1999).
- ³²A. Scherz, H. Wende, P. Pouloupoulos, J. Lindner, K. Baberschke, P. Blomquist, R. Wäppling, F. Wilhelm, and N. B. Brookes, Phys. Rev. B **64**, 180407(R) (2001).
- ³³P. Pouloupoulos, S. Baskoutas, L. F. Kiss, L. Bujdosó, T. Kemény, F. Wilhelm, A. Rogalev, V. Kapaklis, C. Politis, M. Angelakeris, and K. Saksl, J. Non-Cryst. Solids **354**, 587 (2008).
- ³⁴F. Wilhelm, P. Pouloupoulos, G. Ceballos, H. Wende, K. Baberschke, P. Srivastava, D. Benea, H. Ebert, M. Angelakeris, N. K. Flevaris, D. Niarchos, A. Rogalev, and N. B. Brookes, Phys. Rev. Lett. **85**, 413 (2000).
- ³⁵K. Takanashi, S. Mitani, K. Himi, and H. Fujimori, Appl. Phys. Lett. **72**, 737 (1998).
- ³⁶P. Pouloupoulos, F. Wilhelm, H. Wende, G. Ceballos, K. Baberschke, D. Benea, H. Ebert, M. Angelakeris, N. K. Flevaris, A. Rogalev, and N. B. Brookes, J. Appl. Phys. **89**, 3874 (2001).
- ³⁷S. Mirbt, I. A. Abrikosov, B. Johansson, and H. L. Skriver, Phys. Rev. B **55**, 67 (1997).